# Detection of Main Rock Type for Rare Earth Elements (REEs) Mineralization Using Staged Factor and Fractal Analysis in Gazestan Iron-Apatite Deposit, Central Iran

**Fatemeh Soltani[1], Parviz Moarefvand[1]\*, Firouz Alinia[1], Peyman Afzal[2]**

[1] *Department of Mining and Metallurgical Engineering, Amirkabir University of Technology (Tehran Polytechnic), Tehran, Iran*

[2] *Department of Mining Engineering, South Tehran Branch, Islamic Azad University, Tehran, Iran*

*\*Corresponding author, e–mail: parvizz@aut.ac.ir*

## Abstract

Gazestan magnetite-apatite deposit is located in Central Iran and Bafq region, which has been occurred in form of veins, veinlets, and small apatite lenses as well as magnetite in metasomatic rock types such as green chlorite-actinolite rock units. These rocks are situated in the carbonate-volcanic complex of Upper Precambrian-Lower Cambrian Rizo formation. In this study, staged factor analysis and Concentration-Number (C-N) fractal model were used based on core samples for determination of main rock type for Rare Earth Elements (REEs) mineralization. Hence, after normalizing the data by staged factor analysis, the target factors were determined and the factorial map was generated using the C-N fractal modeling. The results showed that the first factor of the sixth step (F1-6) is contained of the REEs with phosphorous. Afterwards, results obtained by the C-N fractal method on the F1-6 indicated that there are five populations for REEs which are compared with different lithological units by evaluation matrix. The evaluation matrix confirmed the compliance of magnetite-apatite units with the high values of mineralization factor. The REEs were accumulated in magnetite-apatite units based on highest Overall Accuracy (OA).

**Keywords**: *Rare Earth Elements (Rees), Staged Factor Analysis, Concentration-Number (C-N) Fractal Model, Gazestan, Iron-Apatite Deposit.*

## Introduction

Metasomatic iron ores are considered significant economically since they are large and major producers of REEs (Laznicka, 2005). Therefore, exploration of the REEs mineralization in metasomatic iron ores has been attended as an exploration priority in recent years. Furthermore, the rising cost of these valuable elements increasingly has led to the recent discoveries of their deposits in developed countries (Sadeghi *et al.,* 2013; Sarparandeh *et al.*, 2017).

The REEs have a variety of applications in modern technology and provide many vital materials related to industry (Humphries, 2011). These elements are classified into light REEs (LREEs) including Ce, Eu, La, Nd, Pr, Sm, and Pm and heavy REEs (HREEs) consisting of Tm, Dy, Er, Gd, Ho, Lu, Tb, Yb, Sc, and Y (Jha, 2014; Simandl, 2014; Emsbo *et al.,* 2015). Recent studies on exploration of the REEs indicate a movement towards using mathematical and statistical modeling methods such as multivariate analysis (Petrosino *et al.*, 2013; Sadeghi *et al.*, 2013; Hellman and Duncan, 2014; Mikhailova *et al.,* 2016; Rahimi *et al.,* 2016; Zaremotlagh & Hezarkhani, 2016).

Several modeling methods have been used in different deposits based on mathematical and statistical methods. However, classical statistical parameters including mean, standard deviation, and histogram and box plot have been employed to determine different geochemical populations (Davis, 1976; Hawkes & Webb, 1979; Afzal, 2010; Yasrebi *et al.,* 2013; Mokhtari *et al.,* 2014, Ghezelbash & Maghsoudi, 2018).

Factor analysis has been used widely as one of the multivariate analysis methods to interpret geochemical data. The major purpose of this analysis is to justify the greatest variability between the observations and variables through linear combination of multiple variables in a space with lower dimensions (Krumbein & Graybill, 1965; Tripathi, 1979; Johnson & Wichern, 2002; Afzal *et al.,* 2016)*.* A large part of variability can be justified by a limited number of new variables, and the coefficients of the initial variables included for calculating each of the principal components may be calculated by either a covariance or correlation matrix (Reimann *et al.,* 2002).

In the results obtained by factor analysis, where either correlation or covariance matrix is used, one observes the emergence of certain noise elements and the absence of mineralization indicator

elements in one factor. Thus, in order to improve the results and modify the effect of noise elements, staged factor analysis has been proposed in a study conducted by Yousefi *et al.,* (2012).

Fractal modeling has been used to separate various geochemical populations as well as barren and mineralized rocks. In this regard, Number-Size (N-S) fractal model was introduced by Mandelbrot (Mandelbrot, 1983); power Spectrum-Area (S-A) technique was presented by Cheng *et al.,* (1994, 2000); Concentration-Distance (C-D) model was proposed by Li *et al.,* (2003); Concentration-Volume (C-V) methodology was suggested by Afzal *et al.,* (2011); power Spectrum-Volume (S-V) fractal method was introduced by Afzal *et al.,* (2012), and Concentration-Number (C-N) model was proposed by Hassanpour & Afzal (2013).

In the present study, a relationship was found between the lithological units and the concentration of REEs in Gazestan iron-apatite deposit (Central Iran) using a combination of stage factor analysis and the C-N fractal model. The correlation was carried out between results and rock types by evaluation matrix.

## Methodology
### *Staged factor analysis*
Multivariate statistical approaches explore the relationships between multiple variables simultaneously. These multivariate methods are often employed to reduce the multivariate dataset so that one can interpret the trend and variability in the dataset using the reduced data (Chandrajith *et al.,* 2001; Helvoort *et al.,* 2005; Gholami *et al.,* 2012).

The staged factor analysis is a multivariate method (Yousefi *et al.,* 2014). This can be used for extracting significant multi-element anomalous signatures. In this approach, In order to find multi-element associations in a geochemical dataset, non-indicator (noisy) elements are identified progressively and are excluded from the analysis until a satisfactory significant multi-element signature is obtained (Yousefi *et al.,* 2012). In order to perform FA, classical PCA (non-robust) was used for extracting the common factors. Subsequently, the Varimax method was used for rotation and factors with eigenvalues of >1 were retained for interpretation (Kaiser 1958). In addition, the threshold value of 0.6 for loadings was considered to extract the significant multi-element geochemical signature of the deposit-type sought.

In the first stage, factor analysis was performed

on the initial data; thereafter, with respect to the considered threshold limit, if there was any element that did not participate in any of the factors, it was deleted and factor analysis would be continued on the data of the remaining elements until all noise elements were eliminated so that there would be no element which did not fit into any of the factors considering the threshold limit. These factors are called clean factors.

In the second stage, those factors having indicator elements were selected for desirable mineralization, and the phases mentioned in the first stage were performed on the elements of these factors. Factor advantages obtained in the last step were utilized to perform exploratory operations (Yousefi *et al.,* 2012; Afzal *et al.,* 2016).

### *Concentration–Number (C–N) fractal Modeling*
Fractal methods can explain the relationships between the results obtained in geological, geochemical, structural, and mineralogical studies. Correspondingly, logarithmic graphs are regarded as tools for isolating and separating geochemical communities in geochemical information. After plotting these logarithmic graphs, wherever the gradient of the curve experiences a sharp change, it means that the geological and mineralogical community has been transformed.

The C–N fractal model was used to define the geochemical background and anomaly threshold values (Mandelbrot, 1983; Deng *et al.,* 2010; Hassanpour & Afzal, 2013). The model has the general form as follow:

$$N(\geq \rho) \propto \rho^{-\beta} \tag{1}$$

Where N ($\geq \rho$) represents the sample number with concentration values greater than the $\rho$ value. $\rho$ and $\beta$ are the concentration of ore element and fractal dimension, respectively. In this method, geochemical data has not undergone pre-treatment and evaluation (Deng *et al.,* 2010; Hassanpour & Afzal, 2013; Afzal *et al.,* 2017).

### *Evaluation matrix*
In order to investigate the correlation of the zones obtained from the fractal method and geological observations, the authors used evaluation matrix. This matrix was proposed first by Caranza (2011), to identify the gold anomalies of stream sediments located in the northwest of Philippines. Using this matrix, the results obtained by the C-N fractal model and geological observations are compared with each other by considering the matrix's

components. Following the calculations of the related matrix, any data with the greatest overall accuracy can be considered as the definitive result with the least error rate.

**Geological setting and mineralization**

Gazestan deposit is located in Yazd province, about 78 km from the city of Bafq and 10 km from the SE of Gazestan village. According to *s*tructural parameters, this deposit belongs to Central Iran and also Bafq-Posht-e Badam metallogenic zone (Afzali *et al*., 2012). The rock types in this area are related to the Rizo series and are consisted of carbonate rocks, shale, tuff, sandstone, and volcanic rocks.

Additionally, intrusions in the form of stocks and dikes with mid-to-basic combinations are occurred in the deposit. The basic dikes are composed of diorite-gabbro and diabase principally.

Green/metasomatic rocks with acidic compositions, which are appeared in green due to metasomatism, are known as the host of iron and phosphate mineralization (Dehghanzade-Bafghi *et al.,* 2017). Metasomatic processes have taken place simultaneously or slightly ahead of mineralization. The intensity of metasomatic processes increases as one approaches the mineralization zone, Fig.1. *(*Parsi Kan Kav Company 2015).
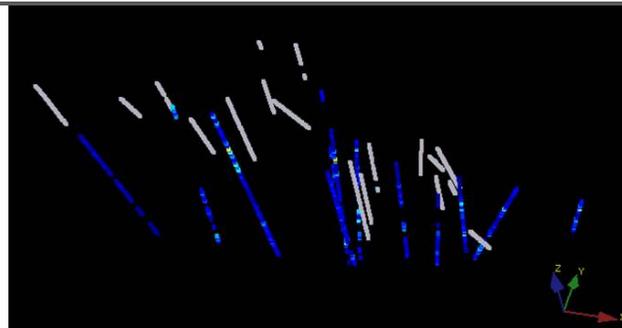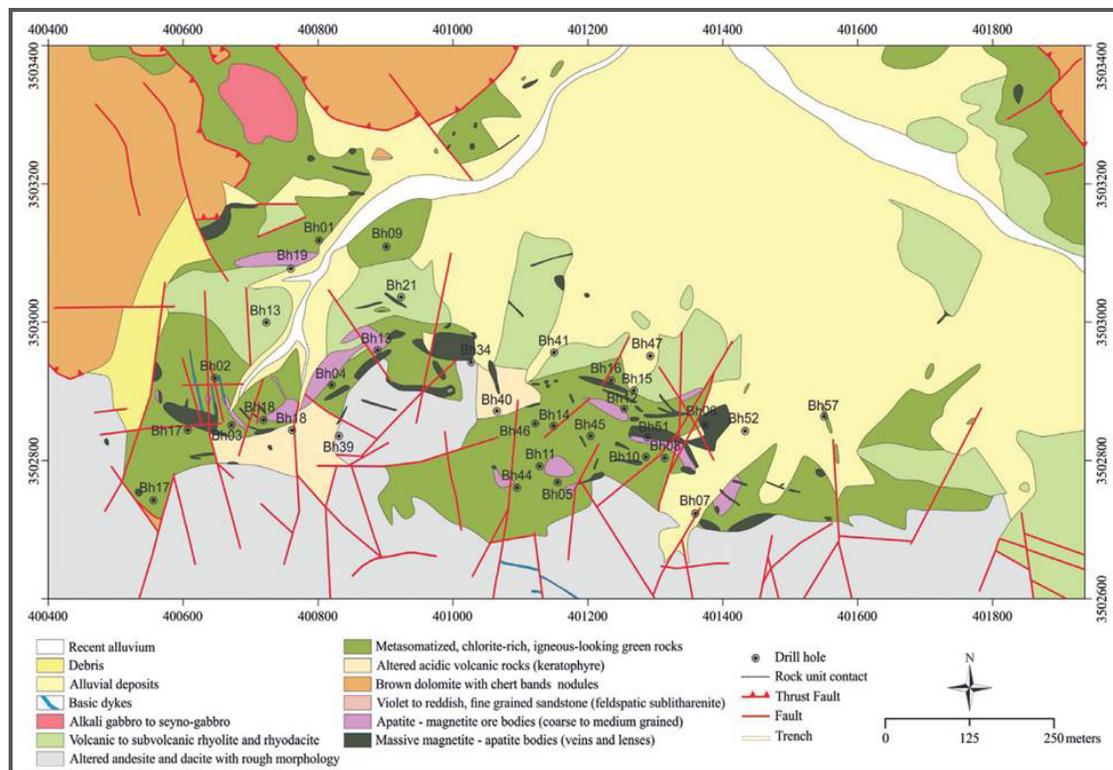


Figure 1. Geological map, Gazestan deposit (modified from Sepehrirad *et al*., 2018), borehole locations are mapped (up) and perspective boreholes locations (down), gray boreholes are not assayed.

Generally, the dominant composition of the rocks in this region is acidic volcanic and microgranite. Except for diorite-gabbro rocks found in the western part of the area, which is considered as a basic mass, as well as some dikes and small stocks. Therefore, the formation of acidic rocks in this deposit is considered to be originated in granitic magma (Afzali *et al*., 2012).

The Gazestan deposit is occurred in the vein form, veinlet and small apatite lenses with magnetite in a green chlorite-actinolite rock unit in the carbonate-volcanic complex of Rizo Formation (Dehganzadeh Bafghi *et al.,* 2019). Moreover, it dates back to the Upper Precambrian- Lower Cambrian periods (Afzali *et al*., 2012).

The green rock unit which includes intrusive volcanic rocks is consisted of andesite, micro-diorite, tuff, as well as mafic-ultramafic rocks which have been altered largely. It seems that veins, magnetite, and apatite lenses have been concentrated in this unit as a pure phase. The apatite mineral is contained of fluorine, and REEs found in this mineral are micro-monazite inclusions and other minerals (Afzali *et al.,* 2012; Parsi Kan Kav Company 2015).

In Gazestan deposit, the mineral is a mixture of magnetite-apatite in various ratios, typically accompanied by quartz and calcite. Quartz and calcite have been formed in the late stages following mineralization. The mineralization zone in Gazestan reaches over 2.4 km long and over 0.7 km wide (Afzali *et al.,* 2012; Parsi Kan Kav Company 2015).

Metasomatism is more evident in volcanic rocks, and the rocks hosting mineralization display sharp metasomatism. The observed metasomatism in this area is mostly occurred in the form of silicic, chloritic, actinolite and argillic types, which are associated with mineralization and have the most development in the area (Dehganzadeh-Bafghi *et al.,* 2019). However, sericitic, potassic, tourmalinic and epidotic metasomatism have also been formed in rock units (Mokhtari, 2015; Sepehrirad *et al.,* 2018).

Diffusion in the study area can be classified into at least 5 groups of faults with the east-west trend, north-south trend, northeast-southwest trend, northwest-southeast trend, and thrust faults. The faults with the east-west trend are the oldest fractures in the region because displacements and variation in dip and strike of the fault that have

been made by other faulting (newer ones) systems. The faults that are in South of studied area, placed volcanic rocks close to the carbonate rocks. Thrust faults have been displaced by the northeastern-southwestern faults (Madani-Esfahani & Asghari, 2013). One of the main functions of these faults is that they have placed hard-eroding rocks such as carbonates and sandstones on soft-eroding units, which are mineral units. Thereby, these faults have prevented further mineral erosion (Parsi Kan Kav Company, 2015)*.*

### Dataset
In the present study, 908 core samples were logged from 12 exploratory boreholes with a total length of 1814 meters. The obtained samples are two meters length. A total of 56 elements including LREEs, HREEs, and total REEs were analyzed by the ACME CEMEX Company using ICP for grade assaying and XRD, and XRF for petrological studies.

In order to determine the distribution of REEs in the study area, statistical parameters including mean, median, variance, histogram, and box plot have been calculated separately in different rocks. Using the data of area, the frequency diagram of LREEs, HREEs and total REEs have been generated so that the target rock unit could be determined for modeling. Thus, using classical statistics, the number of rock units in the region (17) were merged based on the abundance of major minerals and rock units, into seven rock types, as shown in Tables 1 and 2, respectively.

After combining the rock units, the scatter diagram was drawn regarding the ratio of heavy-to-light REEs. Therefore, all the units of rhyodacite, andesite-rhyodacite, and tuff-rhyodacite were converted into rhyodacite. Moreover, all the tuff-andesite units in tuff units, magnetite-albite units, andesite- magnetite, magnetite-diorite, and magnetite-tuff were converted into magnetite unit. Finally, dacite and andesite were combined into dacite.

In order to show the distribution of the concentration values of REEs, a boxplot was drawn for the combined rock units, as shown in (Fig. 2). It is evident that magnetite-apatite units are of the highest value of REEs with a mean of 1362 ppm, and the units of rhyodacite, dacite, and waste rocks have a mean which is equal to 569 ppm, 341 ppm and 380 ppm, respectively.

Table 1. Calculation of statistical parameters in the rock units of Gazestan region (the order of rocks: andesite, dacite, dacite-andesite, diorite, diabase, magnetite, magnetite-albite, magnetite-andesite, magnetite-diorite, magnetite-tuff, slag, rhyodacite, andesite-rhyodacite, tuff-rhyodacite, tuff, andesite-tuff, and waste rock).

| Rock Type | Total Count | Mean of HREE | Median of HREE | Mean of LREE | Median of LREE |
|---|---|---|---|---|---|
| AND | 216 | 208 | 174.6 | 619.4 | 496.4 |
| DAC | 64 | 109.45 | 104.81 | 232.5 | 209.8 |
| DACAN | 2 | 159.16 | 159.16 | 574.19 | 574.19 |
| DIO | 7 | 280 | 191.4 | 1093 | 434 |
| DYA | 2 | 54.8 | 54.800 | 151.52 | 151.2 |
| MAG | 34 | 325.7 | 307.9 | 1154 | 988 |
| MAGALB | 7 | 227.3 | 243.4 | 925 | 992 |
| MAGAN | 104 | 258.6 | 243 | 1041.7 | 952 |
| MAGDI | 1 | 200.2 | 200.2 | 878.03 | 878.03 |
| MAGTUF | 98 | 298.9 | 249.5 | 1107 | 796 |
| OVER | 2 | 599 | 599 | 539 | 539 |
| RYD | 12 | 112.6 | 98 | 312.2 | 210.8 |
| RYDAN | 3 | 203.3 | 134.8 | 789 | 651 |
| RYDTU | 2 | 168.6 | 168.6 | 629 | 629 |
| TUF | 160 | 200.9 | 158.2 | 632.1 | 460.8 |
| TUFAN | 186 | 239.6 | 174.4 | 795.1 | 526.5 |
| WASTE | 8 | 158.7 | 139.3 | 228 | 229.3 |
| Grand Total | 908 | 3804.81 | | 11700.74 | |

Table 2. Calculation of statistical parameters after merging rock units.

| Rock Type | Samples No. | Mean of Total REE (ppm) | Median of Total REE (ppm) | Variance (ppm)² | Mean of HREE (ppm) | Median of HREE (ppm) | Variance (ppm)² | Mean of LREE (ppm) | Median of LREE (ppm) | Variance (ppm)² | LREE /HREE ratio |
|---|---|---|---|---|---|---|---|---|---|---|---|
| AND | 218 | 827 | 689 | 506893 | 208 | 173 | 28662 | 619 | 499 | 305312 | 3.0 |
| DAC | 64 | 342 | 312 | 25946 | 109 | 105 | 1379 | 233 | 210 | 16078 | 2.1 |
| DIO | 7 | 1373 | 606 | 2427355 | 280 | 191 | 40033 | 1093 | 434 | 1845200 | 3.9 |
| MAG | 244 | 1363 | 1163 | 859127 | 283 | 253 | 29478 | 1080 | 921 | 597424 | 3.8 |
| RYD | 17 | 569 | 354 | 188900 | 135 | 104 | 7004 | 434 | 250 | 125934 | 3.2 |
| TUFF | 346 | 941 | 684 | 752432 | 222 | 165 | 29920 | 720 | 497 | 503712 | 3.2 |
| WASTE | 12 | 482 | 380 | 140239 | 215 | 139 | 46887 | 267 | 229 | 25544 | 1.2 |
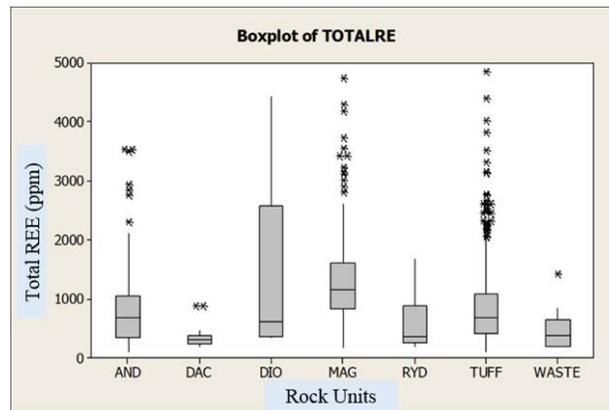


Figure 2. Boxplot of the total REEs in the different rock units.

**Discussion**

The ratio of the distribution of LREEs/HREEs is not the same in rock units. Considering the high variation in the values of variables, logarithm was taken at the base 10 for each of the concentration values of light and heavy REEs, in order to delimit the value range of the axes in the coordinate system, as shown in Fig. 3 and to magnify the variations.

As illustrated in Fig. 2, magnetite units, while having a total average concentration of greater than other units; show a great ratio of light-to-heavy elements since they are located mostly at the top of the one-to-one correspondence line. The ratio of light-to-heavy REEs is equal to 3.8 in magnetite units, and in diorite units, which the number of its samples is quite small, it is equal to 3.9. Moreover, dacite appearing in red are in the lower parts of the diagram, and the ratio of heavy-to-light elements is remarkably high.

The ratio of LREEs/HREEs in rhyodacite, andesite, dacite, tuff and waste rocks are equal to 3.1, 3, 2.1, 3.2 and 1.2, respectively. In other words, this ratio increases significantly with the increase in the total average concentration value in each rock unit.
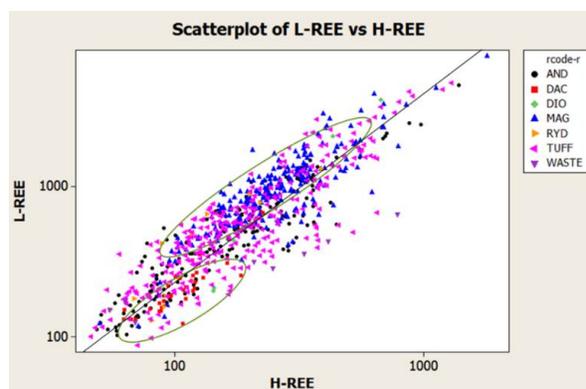


Figure 3. Diagram of distribution of rock units in scatter plot of LREE and HREE

In the current study, in order to extract the main components of mineralization, staged factor analysis was used. Prior to the rotations of this stage, using Normal Score Transformation, all data were converted into normal distribution with the mean of 0 and variance of 1. In the first step, taking into account the threshold limit of 0.6 on the correlation values and the 13 factors, noise elements were deletedwith values lower than the threshold limit of 0.6. In other words, the elements whose values were not higher than the threshold limit were removed from all of these factors. Specifically, in this step, the elements of As, Ba, Bi, Co, Ga, Ni, Sr, W, and Zn were removed as noise or uncorrelated elements.

In the second step of factor analysis, 9 factors were obtained. Here, the noise elements were removed again and the elements such as Cu, In, Mo, Pb, Sb, and Ta were eliminated and 8 factors were obtained. In the next step, the Cr and Tl elements were removed and 7 factors were obtained. In this step, i.e. the fifth step, the Be element was deleted only and the number of factors did not change. No noise element was found in this step. In other words, there is no element that cannot be classified in any of the factors considering the threshold limit of 0.6. Thus, the first phase of the factor analysis was completed and the factors obtained were clean.

In the second phase, we had to choose factors containing the indicator elements of the desirable mineralization. Regarding the study area, considering that the objective is to investigate and identify REEs in the magnetite-apatite rock units in the region, the factors of 1.2 and 3 were considered as the target factors because they were contained of desirable elements, i.e. Fe and REEs. Elements with a threshold lower than 0.6 were removed in this stage. These elements were Ag, Ca, Cd, Cs, Li, Mg, Mn, Nb, and Ti (Table 3). Thus, three factors were obtained in the sixth step, and all the elements (Table 4) had higher values than the threshold limit.

All the remaining elements in the three factors had a minimum correlation of 0.6 with their corresponding factor (Table 4). Therefore, using factor scores, the C-N fractal model was carried out on the first factor of step 6 (F1-6) which had multi-fractal behaviors. The model was used to identify and distinguish REEs in magnetite-apatite rock units in the Gazestan deposit.

In addition, the C-N log-log plot was generated (Fig. 4). The fractal diagram presented in Fig. 4 illustrates the breakpoints between the straight lines in the diagram of values as well as the threshold in order to distinguish rock units and various geological communities.

These breaks are corresponded with 2.77, 1.42, 0.60, and 0.163, respectively. In the last step, there is a distinguished multi-fractal behavior which represents a phase and an enriched rock unit. Since in the Gazestan deposit, the mineral is a mixture of magnetite and apatite, this full-concentration part can be considered to be corresponded with magnetite-apatite rock units.

Table 3. Rotated factor matrix for the fifth stage of the staged factor analysis.

**Fifth stage**

| | Component 1 | 2 | 3 | 4 | 5 | 6 | 7 |
|---|---|---|---|---|---|---|---|
| AG | .140 | -.004 | .204 | -.079 | .128 | 132 | .801 |
| AL | -.444 | -.628 | .039 | .241 | .399 | -143 | -.076 |
| CA | .554 | .184 | -.035 | -.283 | .028 | 643 | .121 |
| CD | .033 | -.004 | -.277 | .025 | -.109 | -009 | .823 |
| CE | .939 | .230 | -.006 | -.066 | .047 | 023 | .023 |
| CS | -.204 | -.200 | .016 | 780 | .194 | -094 | .095 |
| DY | .949 | .157 | .083 | -.025 | -.113 | 062 | .016 |
| ER | .941 | .099 | .069 | -.038 | -.134 | 043 | .020 |
| EU | .932 | .053 | .030 | -.097 | .040 | 100 | .058 |
| FE | .215 | .859 | -.025 | -.136 | .015 | -057 | .031 |
| GD | .959 | .231 | .016 | -.036 | -.087 | 052 | .005 |
| GERMANIUM | .145 | .081 | .891 | -.012 | .003 | 036 | -.032 |
| HREE | .933 | .120 | .216 | -.007 | -.109 | 035 | .008 |
| HF | -.114 | -.815 | -.021 | -.025 | .071 | 079 | .129 |
| HO | .946 | .125 | .047 | -.027 | -.125 | 063 | .018 |
| K | -.345 | -.662 | -.101 | -.016 | .442 | -209 | -.041 |
| LREE | .945 | .229 | .001 | -.066 | -.075 | 051 | .020 |
| LA | .929 | .232 | .006 | -.070 | -.070 | 035 | .032 |
| LI | -.083 | -.004 | .092 | 919 | .098 | -135 | -.030 |

**Fifth stage**

| | Component 1 | 2 | 3 | 4 | 5 | 6 | 7 |
|---|---|---|---|---|---|---|---|
| LU | -.097 | -.058 | -.967 | -.039 | -.058 | 027 | .038 |
| MG | .004 | -.027 | .048 | 930 | -.087 | 059 | -.095 |
| MN | .110 | -.077 | -.056 | -.040 | .014 | 950 | .069 |
| NB | -.203 | -.120 | .056 | -.048 | 826 | 057 | -.038 |
| ND | .945 | .242 | -.005 | -.065 | -.070 | 063 | .003 |
| P | .815 | .382 | -.010 | .048 | .066 | 059 | .077 |
| PR | .941 | .212 | -.030 | -.067 | -.091 | 032 | .040 |
| RB | -.326 | -.640 | -.006 | 165 | .447 | -197 | .035 |
| SC | -.103 | -.515 | .632 | 231 | -.064 | -160 | .128 |
| SM | .955 | .220 | .049 | -.041 | -.103 | 058 | .028 |
| SN | .281 | .718 | .105 | 032 | .089 | -103 | .061 |
| TE | .957 | .179 | .047 | -.036 | -.097 | 072 | .013 |
| TH | .646 | -.329 | .133 | -.350 | -.255 | -010 | .099 |
| TI | -.164 | .075 | .053 | 202 | 885 | 019 | .067 |
| TM | -.097 | -.058 | -.967 | -.039 | -.058 | 027 | .038 |
| TOTALREE | .962 | .208 | .050 | -.055 | -.077 | 043 | .020 |
| U | .648 | -.417 | .171 | -.258 | -.053 | -108 | .111 |
| V | .259 | .885 | .022 | -.023 | .106 | 042 | .052 |
| YE | .912 | .045 | .073 | -.062 | -.165 | 092 | .026 |

Table 4. Rotated factor matrix for the sixth stage of the staged factor analysis.

**Sixth stage**

| | Component 1 | 2 | 3 |
|---|---|---|---|
| AL | -.451 | .706 | .077 |
| CE | .920 | .310 | -.005 |
| DY | .938 | .244 | .084 |
| ER | .938 | .187 | .069 |
| EU | .926 | .126 | .030 |
| FE | .143 | .864 | -.031 |
| GD | .937 | .314 | .018 |
| GERMANIUM | .138 | .102 | 889 |
| HREE | .922 | .206 | .221 |
| HF | -.031 | .820 | -.027 |
| HO | .939 | .213 | .049 |
| K | -.340 | -.738 | -.066 |
| LREE | .926 | .310 | .001 |
| LA | .910 | .310 | .008 |

**Sixth stage**

| | Component 1 | 2 | 3 |
|---|---|---|---|
| LU | -.079 | -.066 | -.973 |
| ND | .924 | .324 | -.004 |
| P | .765 | .435 | .000 |
| PR | .926 | .292 | -.030 |
| RB | -.336 | -.715 | .039 |
| SC | -.069 | -.526 | .652 |
| SM | .938 | .305 | .050 |
| SN | .197 | .717 | .129 |
| TB | .944 | .266 | .049 |
| TH | .726 | -.248 | .097 |
| TM | -.079 | -.066 | -.973 |
| TOTALREE | .944 | .291 | .052 |
| U | .705 | -.361 | .154 |
| V | .173 | .886 | .023 |
| YB | .921 | .138 | .069 |
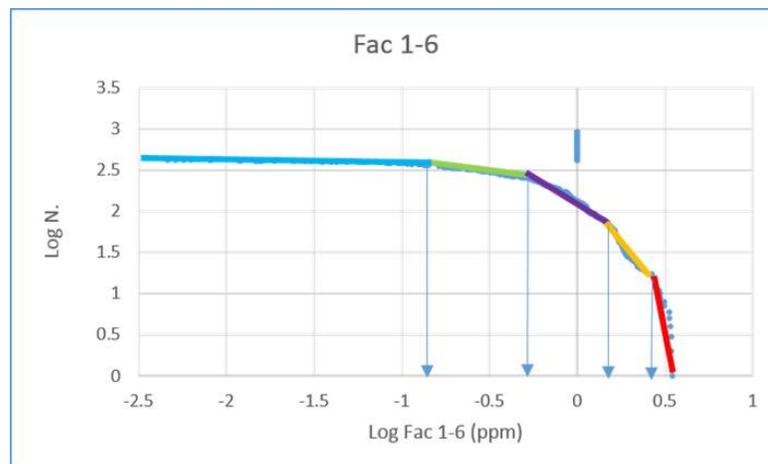


Figure 4. Logarithmic curve of concentration–number of the scores of the first factor in the sixth step of staged factor analysis

Using the evaluation matrix (Table 5), the present study attempted to investigate the correspondence of the Magnetite-Apatite zone obtained from the concentration-number fractal method and geological observations. Using this matrix, the results achieved from the multi-fractal model will be compared with each other by considering the matrix's components.

After calculating the desired matrix, any datum that has the greatest overlap with the results of the concentration-number fractal model will have the highest overall accuracy and can be seen as a definitive result with the lowest error rate. The matrix was also provided for Andesite and tuff

rocks. Comparing the results of andesite and tuff with those of Magnetite-Apatite illustrates that the errors are significantly higher and, as expected it confirms that the desired range of high REE values has compliance mostly with Magnetite-Apatite.

**Conclusion**

The main mineralization is occurred in magnetite-apatite units in the Gazestan deposit. However, according to statistical studies conducted in the present research, there are also significant full-concentration quantities of rare elements in other units of this deposit such as tuff and andesitic unit.

Table5. Overall accuracy, Type 1 and Type 2 errors calculated to match the first factor model of the sixth step with the geological model (magnetite-apatite)

| Geological Model | | | |
|---|---|---|---|
| Outside the zone(magnetite-apatite) | Within the zone(magnetite-apatite) | | |
| False positive(B)= 51 | True positive(A)= 26 | Within the zone1.42037-3.47384 | Fractal model |
| True negative(D) = 612 | False negative (C) = 218 | Outside the zone 1.42037-3.47384 | |
| Error type2 = 0.07 | Error type1=0.893 | | |
| overall accuracy = 70% | | | |

Table 6. Overall accuracy, Type 1 and Type 2 errors calculated to match the first factor model of the sixth step with the geological model (Andesite)

| Geological Model | | | |
|---|---|---|---|
| Outside the zone(Andesite ) | Within the zone(Andesite ) | | |
| False positive(B)=67 | True positive(A)= 10 | Within the zone1.42037-3.47384 | Fractal model |
| True negative(D) = 622 | False negative (C) = 208 | Outside the zone 1.42037-3.47384 | |
| Error type2 = 0.1 | Error type1=0.95 | | |
| overall accuracy =69% | | | |

Table 7. Overall accuracy, Type 1 and Type 2 errors calculated to match the first factor model of the sixth step with the geological model (Tuff)

| Geological Model | | | |
|---|---|---|---|
| Outside the zone (Tuff ) | Within the zone (Tuff ) | | |
| False positive(B)= 37 | True positive(A)= 40 | Within the zone1.42037-3.47384 | Fractal model |
| True negative(D) = 525 | False negative (C) = 305 | Outside the zone 1.42037-3.47384 | |
| Error type2 = 0.06 | Error type1 = 0.88 | | |
| overall accuracy = 62 % | | | |

Based on the results, with the increase in the concentration of rock units, the ratio of the concentration of light to heavy REEs increases significantly. In other words, the share of light elements in apatite-magnetite units is far more than those of rhyodocite and dacite, which have low levels of REEs.

Based on multivariate statistical studies, using staged factor analysis demonstrated desirable efficiency in separating elements irrelevant (noise) to mineralization. This suggestion becomes more important dealing with a large number of similar variables, in which was the case of the present study (56 concentration variables), that would disrupt the multivariate identification system where they are used all at once. Applying this technique, inefficient elements in the process of separation were removed practically from the dataset. Consequently, having refined information, more accurate separation of rock communities was carried out on the factor obtained from the new data based on the concentration-number fractal model.

Using a verification matrix, this separation led to a quantitative and modeled distinction between magnetite-apatite units as the main component of mineralization in Gazestan.

## Acknowledgment

## References

Afzal, P., Ahmadi, K., Rahbar, K., 2017. Application of fractal-wavelet analysis for separation of geochemical anomalies. Journal of African Earth Sciences. 128: 27–36.

Afzal, P., Eskandarnejad Tehrani, M., Ghaderi, M., 2016. Delineation of supergene enrichment, hypogene and oxidation zones utilizing staged factor analysis and fractal modeling in Takht-e-Gonbad porphyry deposit, SE Iran. Journal of Geochemical Exploration, 119–127.

Afzal, P., Fadakar Alghalandis, Y., Khakzad, A., Moarefvand, P., Rashidnejad Omran, N. 2011. Delineation of mineralization zones in porphyry Cu deposits by fractal concentration–volume modeling. Journal of Geochemical Exploration; 108: 220–232.

Afzal, P., Fadakar Alghalandis, Y., Moarefvand, P., Rashidnejad Omran, N., Asadi Haroni, H., 2012. Application of power-spectrum-volume fractal method for detecting hypogene, supergene enrichment, leached and barren zones in Kahang Cu porphyry deposit, Central Iran. Journal of Geochemical Exploration. 112: 131–138.

Afzal, P., Harati, H., Fadakar Alghalandis, Y., Yasrebi, A.B., 2013. Application of spectrum–area fractal model to identify of geochemical anomalies based on soil data in Kahang porphyry-type Cu deposit, Iran. Chem. Journal of Chemie der Erde - Geochemistry. 73: 533–543.

Afzal, P., Khakzad, A., Moarefvand, P., 2010. Geochemical anomaly separation by multifractal modeling in Kahang (Gor Gor)porphyry system, Central Iran, Journal of Geochemical Exploration, 34–46.

Afzal, P., Mirzaei, M., Yousefi, M., 2016. Delineation of geochemical anomalies based on stream sediment data utilizing fractal modeling and staged factor analysis. Journal of African Earth Sciences.

Afzali, S., Nezafati, N., Ghaderi, M., 2012. "The Study of Fluid Shortcuts and Stable Isotope of Magnetite-Apatite of Gazestan Deposit in Central Iran." Journal of Geosciences. 101: 35-45.

Carranza, E.J.M., 2011. Analysis and mapping of geochemical anomalies using logratio-transformed stream sediment data with censored values. Journal of Geochemical Exploration. 110: 167-185.

Chandrajith, R., Dissanayake, C.B., Tobschall, H.J., 2001. Application of multi-element relationships in stream sediments to mineral exploration: a case study of Walawe Ganga Basin, Sri Lanka. Journal of Applied Geochemistry. 16: 339–350.

Cheng, Q, Agterberg F.P., Ballantyne, S.B., 1994. The separation of geochemical anomalies from background by fractal methods. Journal of Geochemical Exploration. 51:109–130.

Cheng, Q., Xu, Y., Grunsky, E., 2000. Integrated spatial and spectrum method for geochemical anomaly separation. Natural Resources Research, 9: 43-51.

Davis, J.C., 2002. Statistics and Data Analysis in Geology, 3th ed. John Wiley & Sons Inc, New York. 638 p.

Dehghanzadeh Bafghi, A.A., Kohsary, A.H., 2017. Identifying Rare Earth Elements and Thorium and Uranium in Iron Oxide–Apatite Deposit of Gazestan Bafgh, Southeast of Iran. Journal of Mining Science, 161-175.

Deng, J., Wang, Q., Yang, L., Wang, Y., Gong, Q., Liu, H., 2010. Delineation and explanation of geochemical anomalies using fractal models in the Heqing area, Yunnan Province, China. Journal of Geochemical Exploration. 105: 95–105.

Emsbo, P., McLaughlin, P.I., Breit, G.N., du Bray, E.A., Koenig, A.E., 2015. Rare earth elements in sedimentary phosphate deposits: solution to the global REE crisis? Journal of Gondwana Research.

Final Report on Advanced Exploration in Mining Area of Gazestan. Parsi Kan Kav Engineering Company. 2015.

Ghezelbash, R., Maghsoudi, A., 2018. Comparison of U-spatial statistics and C–A fractal models for delineating anomaly

patterns of porphyry-type Cu geochemical signatures in the Varzaghan district, NW Iran. Journal of Comptes Rendus Geoscience, 350(4): 180-191.

Gholami, R., Moradzadeh, A., Yousefi, M., 2012. Assessing the performance of independent component analysis in remote sensing data processing. J. Indian Soc.Remote Sens. 40: 577–588.

Hassanpour, Sh., Afzal, P., 2013. Application of concentration–number (C–N) multifractal modeling for geochemical anomaly separation in Haftcheshmeh porphyry system, NW Iran. Arabian Journal of Geosciences.

Hawkes, R., Webb, H. 1979. Geochemistry in mineral exploration, 2nd edn. Academic Press, New York, 657 p.

Hellman, P. L., Duncan, R. K., 2014. Evaluation of rare earth element deposits. Applied Earth Science.

Humphries, M., 2011. Rare earth elements: The global supply chain, Specialist in energy policy, Congressional research service.

Helvoort, P., J., V., Filzmoser, P., Van Gaans, P.F.M., 2005. Sequential factor analysis as a new approach to multivariate analysis of heterogeneous geochemical datasets: an application to a bulk chemical characterization of fluvial deposits (Rhine–Meuse delta, The Netherlands). Applied Geochemistry. 20: 2233–2251.

Jha, A., 2014. Rare Earth Materials: Properties and Applications. CRC Press.

Johnson, R.A., Wichern, D.W., 2002. Applied Multivariate Statistical Analysis, 5th ed. Prentice Hall, Upper Saddle River, New Jersey.

Kaiser, H.F., 1958. The varimax criteria for analytical rotation in factor analysis. Psychometrika 23: 187–200.

Krumbein, W.C., Graybill, F.A., 1965. An Introduction to Statistical Models in Geology. McGraw-Hill,

Laznicka, P., 2005. Giant Metallic Deposits Future Sources of Industrial Metals. SpringerVerlag. 732 pp.

Li, C., Ma, T., Shi, J., 2003. Application of a fractal method relating concentrations and distances for separation of geochemical anomalies from background. Journal of Geochemical Exploration.77: 167–175.

Madani Esfahani, N., Asghari, O., 2013. Fault Detection in 3-D by Sequential Gaussian Simulation of Rock Quality Designation (RQD), Case Study: Gazestan Phosphate Ore Deposit (Central Iran). Arabian Journal of Geosciences. 6 (10): 3737–3747.

Mandelbrot, B.B., 1983. The Fractal Geometry of Nature. W. H. Freeman, San Fransisco. 468 p.

Mikhailova, Julia A., Kalashnikov, Andrey O., 2016. 3D mineralogical mapping of the Kovdor phoscorite–carbonatite complex (Russia). Miner Deposita. 51: 131–149.

Mokhtari, A.R., Roshani Rodsari, P., Fatehi, M., Shahrestani, Sh., Pournik, P., 2014. Geochemical prospecting for Cu mineralization in an arid terrain-central Iran. Journal of African Earth Sciences 100: 278-288. New York.

Mokhtari, A.R., 2015. Posht-e-Badam Metallogenic Block (Central Iran): A suitable zone for

REE mineralization, Central European Geology, 58 (3): 199–216.

Paola Petrosino, P., Sadeghi, M., Albanese, S., Andersson, M., 2013. REE contents in solid sample media and stream water from different geological contexts: Comparison between Italy and Sweden. Journal of Geochemical Exploration, 133: 176–201.

Rahimi E., Maghsoudi A., Hezarkhani, A., 2016. Geochemical investigation and statistical analysis on rare earth elements in Lakehsiyah deposit, Bafq district. Journal of African Earth Scinences.

Reimann, C., Filzmoser, P., Garrett, R.G., 2002. Factor analysis applied to regional geochemical data: 301 problems and possibilities. Applied geochemistry. 17: 185–206.

Sadeghi, M., Morris, G. A., Carranza, E. J. M., Ladenberger, A., Andersson, M., 2013. Rare earth element distribution and mineralization in Sweden: An application of principal component analysis to FOREGS soil geochemistry. Journal of Geochemical Exploration, 133: 160–175.

Sarparandeh, M., Hezarkhani, A, 2017. Studying distribution of rare earth elements by classifiers, Se-Chahun iron ore, Central Iran. Acta Geochimica. 36(2): 232–239

Sepehrirad, R., Alirezaei, S., Azimzadeh A.M., 2018. Hydrothermal alteration in the Gazestan iron ore deposit; comparison to other Kiruna-type iron deposits in Central Iran, Geological Survey and Mineral Exploration of Iran. 27 (108): 257-268.

Simandl, G., 2014. Geology and market-dependent significance of rare earth element resources Mineral. Deposita, 49: 889–904.

Tripathi, V.S., 1979. Factor analysis in geochemical exploration. Journal of Geochemical Exploration 11: 263–275.

Yasrebi, A.B., Afzal, P., Wetherelt, A., Foster, P., Esfahanipour, R., 2013. Correlation between Geological and Concentration-Volume Fractal Models for Cu and Mo Mineralised Zones Separation in Kahang Porphyry Deposit, Central Iran. Geologica Carpathica 64 (2): 153—163.

Yousefi, M., Kamkar-Rouhani, A., Carranza, E.J.M., 2012. Geochemical mineralization probability index (GMPI): A new approach to generate enhanced stream sediment geochemical evidential map for increasing probability of success in mineral potential mapping. Journal of Geochemical Exploration. 115: 24–35.

Yousefi, M., Kamkar-Rouhani, A., Carranza, E.J.M., 2014. Application of staged factor analysis and logistic function to create a fuzzy stream sediment geochemical evidence layer for mineral prospectivity mapping. Geochemistry:

Exploration, Environmental, Analysis. 14: 45-58.

Zaremotlagh, S., Hezarkhani, A., 2016. A geochemical modeling to predict the different concentrations of REE and their hidden patterns using several supervised learning methods: Choghart iron deposit, bafq, Iran. Journal of Geochemical Exploration 165: 35–48.